Computers, Materials & Continua

Tech Science Press

https://doi.org/10.32604/cmc.2026.078105

ARTICLE

Energy-Efficient ASTAR-RIS and WPT-Assisted Task Offloading and Content Caching for WSNs

Xiaoping Yang[1,*], Songjie Yang[2], Junqi Long[1], Quanzeng Wang[3], Bin Yang[4], Xiaofang Cao[5] and Guochao Qi[6]

[1]College of Computer Science, Beijing University of Technology, Beijing, China
[2]National Key Laboratory of Wireless Communications, University of Electronic Science and Technology of China, Chengdu, China
[3]China Unicom Software Research Institute, Beijing, China
[4]Center for Strategic Assessment and Consulting, Academy of Military Science, Beijing, China
[5]School of Business, Beijing Wuzi University, Beijing, China
[6]Beijing Institute of Computer Technology and Application, Beijing, China

*Corresponding Author: Xiaoping Yang. Email: yangxiaoping7@emails.bjut.edu.cn

Received: 24 December 2025; Accepted: 12 February 2026; Published: 08 May 2026

ABSTRACT: The rapid proliferation of latency-sensitive applications, coupled with the limitations of service range, has driven the integration of aerial simultaneously transmitting and reflecting reconfigurable intelligent surfaces (ASTAR-RIS) and task offloading to enhance both communication and computational efficiency in wireless sensor networks (WSNs). However, in WSNs, conventional ASTAR-RIS-assisted task offloading faces critical limitations, including restricted endurance, underutilized network caching and computing resources, and inefficient resource allocation within the optimization framework. To overcome these challenges, this paper integrates wireless power transfer (WPT) technology and proposes a novel energy-efficient ASTAR-RIS and WPT-assisted task offloading and content caching framework for WSNs. Furthermore, we construct a minimization problem that jointly optimizes content caching, energy harvesting time, task offloading, and STAR-RIS resource allocation decisions to minimize energy consumption. Due to its inherently non-convex structure, the problem is addressed by separating it into four subproblems involving content caching, energy harvesting time, task offloading, and STAR-RIS resource allocation decisions. To address the above subproblems, a joint deep reinforcement learning (DRL)–successive convex approximation (SCA) based scheme is designed, which iteratively achieves the solution and attains near-optimal performance with relatively low computational complexity. Simulation results show that the proposed framework achieves more efficient resource utilization in WSNs and markedly lowers the total energy consumption of the system.

KEYWORDS: Aerial simultaneously transmitting and reflecting reconfigurable intelligent surfaces; task offloading; wireless sensor networks; wireless power transfer; content caching

1 Introduction

With the rapid advancement of wireless sensor networks (WSNs), the explosive increase in the number of sensor devices has dramatically boosted the requirements for high transmission rates and ultra-low latency services [1]. This growth is partly due to emerging service paradigms, e.g., autonomous driving, augmented and virtual reality, and online game applications [2]. These emerging applications impose a great challenge for traditional networks based on centralized cloud-computing frameworks [3]. In order to effectively tackle this challenge, mobile edge computing (MEC) has arisen as a favorable solution by

extending the computational capacity from the central cloud to the network edge cloud, which allows mobile devices (MDs) to offload workloads to proximate edge servers, cutting local energy expenditure and relieving computational burden [4]. Nevertheless, in traditional MEC systems, edge servers and base stations (BSs) are installed at fixed locations on the ground, which have two main disadvantages [5]. First, the quality of service cannot be guaranteed for MDs in remote areas or those blocked by obstacles. Second, terrestrial MEC links often experience severe signal attenuation, so uplink transmission performance remains unsatisfactory.

Unmanned aerial vehicle (UAV) assisted task offloading in WSNs, leveraging the controllable flexibility of UAVs, offers a promising solution to address the aforementioned challenges [6]. To take advantage of the superiority of the UAV, the lightweight edge server can be installed on the UAV, bringing computation physically closer to the users and thus boosting overall system performance [7]. Although UAV-assisted task offloading can effectively enhance the computing capacity of WSNs, existing UAV-assisted offloading frameworks are designed to adapt to uncontrollable random wireless channels, which significantly limits the task offloading efficiency [8]. To break this performance bottleneck caused by random wireless channels, the technology of simultaneously transmitting and reflecting reconfigurable intelligent surface (STAR-RIS) provides a promising solution [9]. STAR-RIS is capable of splitting the incoming signal into two parts, with one portion being reflected back in the direction of the incident signal and the other segment being transmitted in the opposite direction, providing omnidirectional 360° coverage [10]. Therefore, integrating the STAR-RIS into the UAV-assisted offloading systems is viewed as a win-win strategy, simultaneously strengthening link reliability and boosting edge-computing performance. Unfortunately, both UAVs and STAR-RIS face their respective deficiencies, e.g., UAVs are constrained by finite endurance, and the application of STAR-RIS still faces limited coverage owing to its fixed deployment.

To address these challenges, mounting STAR-RIS on the UAV to constitute the aerial STAR-RIS (ASTAR-RIS) to support terrestrial communication is a promising approach [11]. Compared with the UAV-carried server scheme, the ASTAR-RIS architecture constitutes a seamless upgrade to the traditional land server-based task offloading system without the need for routing modifications and system reconstruction [12]. As the STAR-RIS is lighter than an onboard edge server, it imposes only a negligible energy burden on the UAV [13]. In parallel, to further boost the sustainability and computing capacity of the UAV-assisted task offloading system, the wireless power transfer (WPT) technology has been proposed as a promising solution [14]. In this framework, the UAV and user devices harvest energy from radio frequency (RF) signals transmitted by a dedicated energy source and then utilize the harvested energy to support the local processing or task offloading of tasks [15].

1.1 Related Works

1.1.1 UAV-Assisted Task Offloading for WSNs

In recent years, although MEC has provided an effective means to enhance WSN computing capabilities, traditional deployment strategies that place MEC servers near ground BSs or access points (APs) often suffer from limited service coverage [5]. To address this shortcoming, UAVs have emerged as promising offloading assistants, owing to their inherent advantages such as exceptional mobility and flexibility [16–18]. Xu et al. [16] proposed a new system with the cooperation of multiple ground servers and one UAV server, which makes full use of the mobility of UAVs to compensate for the weakness of signal fading between ground servers and users and enhances the computing power of the network. Although UAVs can effectively improve the computing capacity of WSNs, the existing UAV-assisted task offloading frameworks are designed by adapting to uncontrollable random wireless channels, which seriously limits the task offloading efficiency.

1.1.2 STAR-RIS-Assisted Task Offloading for WSNs

STAR-RIS technology has recently emerged as a promising solution to address these challenges [9,19]. STAR-RIS splits the incoming signals into two distinct parts, one reflected back toward the incident direction and another transmitted toward the opposite direction, providing omnidirectional 360° coverage. Some studies mount the STAR-RIS on building façades to assist either the uplink offloading of tasks from ground users to an edge node or the downstream forwarding from the edge node to a terrestrial BS [20–22]. Eghbali et al. [20] proposed an integrated sensing and communication framework, and STAR-RIS, fixed on the exterior walls of buildings, enhances the channel performance between UAVs and users, effectively assisting UAVs in providing high-quality services to mobile users and sensing targets. Yang et al. [22] investigated energy-aware task offloading for rotatable STAR-RIS-enhanced MEC, jointly optimizing the STAR-RIS rotation angle and computing resource allocation to reduce system energy consumption. Despite the notable performance improvements offered by these designs, two key drawbacks persist. First, conventional, fixed-location STAR-RIS deployment severely restricts coverage and flexibility. Second, UAVs that simultaneously perform edge computing and relay functions must carry complex and heavy hardware.

1.1.3 ASTAR-RIS-Assisted Task Offloading for WSNs

To fully exploit the high-mobility potential of UAVs, Li et al. [23] have proposed mounting RIS on UAV platforms, enabling flexible aerial deployment to significantly enhance link quality. However, conventional RIS architectures are constrained by a reflection-only mode and inherently provide coverage over only a half-space region. To overcome this limitation, an aerial STAR-RIS (ASTAR-RIS) architecture that integrates STAR-RIS with UAVs has been proposed. Compared with fixed STAR-RIS deployments mounted on building facades, the ASTAR-RIS architecture offers superior deployment flexibility and practical value, thereby effectively improving task offloading efficiency in WSNs [11]. Aung et al. [11] explored the architecture of mounted STAR-RIS on the UAV, which effectively expanded the service coverage of the system by fully leveraging the mobility of UAVs and the channel control capability of STAR-RIS and minimizing the overall energy consumption of IoT devices and ASTAR-RIS. Collectively, these works confirm that the ASTAR-RIS architecture can dynamically reposition to optimize channel conditions and extend network service coverage, minimizing the system's energy consumption.

1.2 Motivation and Contributions

Motivated by these key technologies, the ASTAR-RIS architecture has emerged as a promising solution for enhancing communication performance in WSNs. Although ASTAR-RIS-assisted offloading systems can substantially extend service coverage and improve wireless transmission quality, several critical challenges remain. First, the limited energy storage capacity of UAV batteries continues to impose a strict bound on their flight endurance. Second, the intrinsic caching and computing capabilities are not fully exploited, resulting in inefficient utilization of network resources and a deterioration in overall system performance. Addressing these issues provides the core motivation for this work. The main contributions of this paper are summarized as follows:

- In this paper, we propose an energy-efficient ASTAR-RIS and WPT-assisted task offloading and content caching framework aimed at minimizing the system energy consumption for WSNs. The proposed framework delivers adaptive and continuous computing and caching services. Moreover, we introduce the ASTAR-RIS architecture, where the STAR-RIS is mounted on the UAV to enable dynamic positioning and to optimize communication channels. Lastly, utilize WPT technology, enabling UAVs and user devices to harvest energy from dedicated RF signals, significantly improving the system's self-sustainability and computational capacity.

- Due to the minimization problem of energy consumption, the inherently non-convex structure, the problem is addressed by separating it into four subproblems involving content caching, energy harvesting time, task offloading, and STAR-RIS resource allocation decisions. To address the above subproblems, a joint deep reinforcement learning (DRL)–successive convex approximation (SCA) based scheme is designed, which iteratively achieves the solution and attains near-optimal performance with relatively low computational complexity.
- Simulation results show that the proposed energy-efficient ASTAR-RIS and WPT-assisted task offloading and content caching framework achieves more efficient resource utilization in WSNs and markedly lowers the total energy consumption of the system, outperforming benchmark solutions, particularly in scenarios with limited network resources or computationally intensive tasks.

The remainder of this paper is structured as follows. Section 2 begins by presenting the system model and formulating the core optimization problem. Building upon this foundation, Sections 3 and 4 detail the proposed optimization algorithm and its iterative solution procedure. Subsequently, the convergence analysis of the devised DRL-SCA algorithm is provided in Section 5. Section 6 then presents the simulation setup and discusses the corresponding numerical results. Finally, the paper concludes with a summary in Section 7.

2 System Model and Problem Formulation

This section presents the system models for the proposed ASTAR-RIS and WPT-assisted WSNs, including network, communication, energy harvesting, task offloading, and caching models, as well as an analysis of system energy consumption. Building on these models, we then formulate the corresponding optimization problem for minimizing the total system energy consumption.

2.1 Network Description

As illustrated in Fig. 1, we consider an ASTAR-RIS and WPT-assisted WSN comprising a single BS, a UAV integrated with a STAR-RIS, and a set of single-antenna user devices (UDs) [24]. The direct links between the UDs and the BS are assumed to be blocked. Consequently, a STAR-RIS is introduced to facilitate connectivity by jointly reflecting and transmitting signals. It is implemented as a uniform planar array (UPA) containing $M_c \times M_r$ passive units and operates in the energy-splitting (ES) mode [25] for flexible beam manipulation. Service provision for the UD set $\mathcal{D} = \{1, 2, \ldots, D\}$ is supported by both the BS b and the UAV u. In particular, a computing server and an RF energy transmitter are integrated at the BS so that it can broadcast wireless energy to the UAV and UDs and execute computational tasks, while the UAV and UDs have rechargeable batteries, energy harvesting (EH) circuit components, and computing servers that can store the harvested energy to power their operation. Moreover, caching servers are integrated at the BS and the UAV so that they can cache computational results in advance and reduce computing resource consumption. Assuming that the transceivers of both UDs and the UAV operate in half-duplex mode, task offloading and local processing can only start after the EH phase is completed, as per the harvest-then-transmit protocol [26]. To ensure energy sustainability, the total energy consumed by the UAV and each UD for task processing and offloading is constrained to be no greater than the amount of energy harvested from the RF signals [27].

In the task scenario description, when the task application programs and their related parameter data are cached by the UAV u or BS b, the system directly processes the caching task and returns the task results. By contrast, in scenarios where the relevant data are not stored in the system cache, we adopt a partial offloading strategy for computation tasks that are sensitive to latency. This task offloading framework enables parallel processing of tasks across three entities: the UDs, UAV u, and BS b.

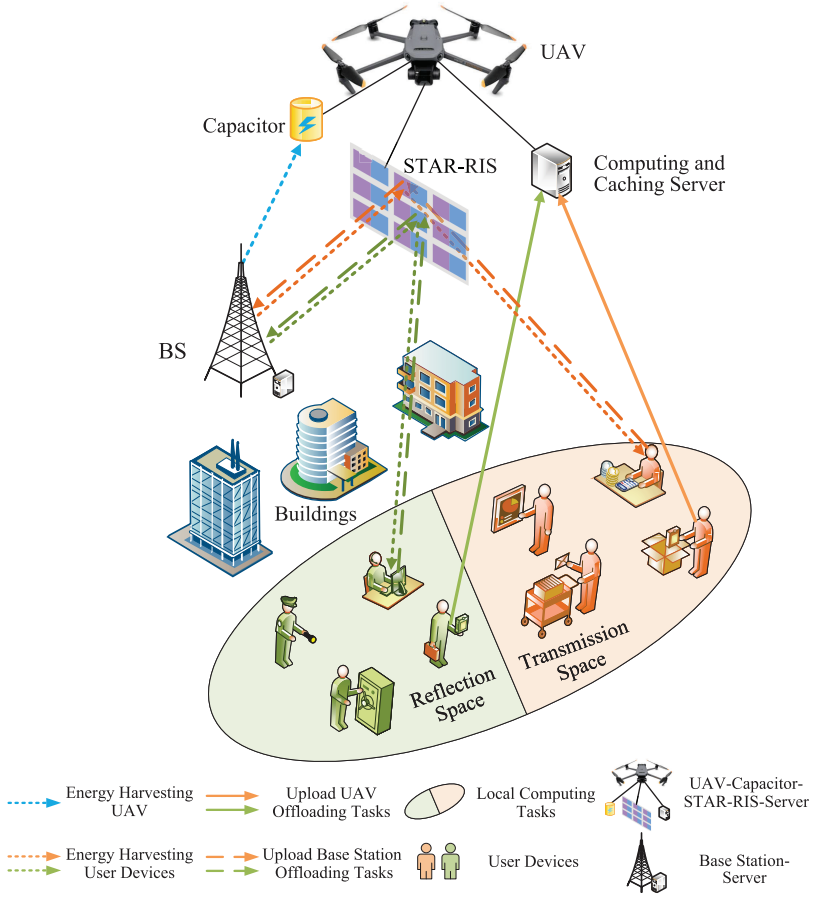

Figure 1: System model of the ASTAR-RIS and WPT-assisted WSNs.

In this paper, we consider a quasi-static service period during which the UAV hovers at a fixed location. This modeling choice is adopted to keep the problem tractable and to highlight the proposed WPT-assisted ASTAR-RIS framework. Note that the joint optimization of UAV hovering location with STAR-RIS passive beamforming, task offloading, and content caching has been thoroughly investigated in our prior work [28]. Therefore, we treat the hovering location as a given parameter and focus on the novel joint optimization of WPT-enabled energy harvesting time, STAR-RIS resource allocation, content caching, and task offloading decisions. It is worth noting that the proposed framework exhibits inherent adaptability to dynamic channel conditions through the real-time reconfiguration of STAR-RIS passive beamforming. The iterative DRL-SCA algorithm updates resource allocation decisions based on current channel state information, enabling the system to maintain energy efficiency under time-varying wireless environments.

2.2 Communication Model

We first derive the uplink data rates corresponding to task offloading from UDs to the UAV and BS, as well as the channel gains associated with the BS's wireless energy broadcast to the UAV and UDs. It is presumed that UDs remain relatively stationary throughout the task offloading process. To characterize the positions of UD d, UAV u, STAR-RIS, and BS b, a three-dimensional (3D) cartesian coordinate system is constructed. Specifically, the locations of UD d and BS b are represented by the vectors $\boldsymbol{r}_d = (x_d, y_d, 0)$ and $\boldsymbol{r}_d = (x_d, y_d, 0)$, respectively. Additionally, we suppose that in each time slot, the UAV u hovers at a fixed position to deliver services to the UDs. Let the 3D coordinate of the UAV u and the (m_c, m_r)-th

STAR-RIS element are denoted as $\boldsymbol{r}_u = (x_u, y_u, z_u)$ and $\boldsymbol{r}_{(m_c,m_r)} = (x_{(m_c,m_r)}, y_{(m_c,m_r)}, z_{(m_c,m_r)})$, respectively. All considered links, between UD d and each STAR-RIS element, UD d and UAV u, and each STAR-RIS element and BS b, are all modeled as line-of-sight (LoS) channels and follow a free-space path-loss model [29]. Consequently, the complex channel gain between any two distinct nodes i and i' (where $i \in \{d, (m_c, m_r), b\}$, $i' \in \{u, (m_c, m_r), b, d\}$) is expressed as $h_{i,i'} = \sqrt{q_0} S_{i,i'}^{-2}$, where q_0 is the reference received power at a reference distance of one meter under unit transmit power, and $S_{i,i'}$ denotes the Euclidean distance between nodes i and i', given by $S_{i,i'} = \sqrt{(x_i - x_{i'})^2 + (y_i - y_{i'})^2 + (h_i - h_{i'})^2}$.

In the system, an orthogonal frequency-division multiple access (OFDMA) scheme is considered to eliminate the intra-cell interference from nodes. Consequently, for the wireless link from node i to node i', the signal-to-noise ratio (SNR) is given by $\gamma_{i,i'} = \frac{P_i |h_{i,i'}|^2}{\sigma_{i,i'}^2}$. The P_i denotes the node i's transmit power, and $\sigma_{i,i'}^2$ is the noise variance at the receiver, which is assumed to be constant variance for the considered links. Accordingly, this SNR then yields the achievable transmission rate $R_{i,i'} = B_{i,i'} \log_2 (1 + \gamma_{i,i'})$, with $B_{i,i'}$ denoting the allocated bandwidth.

2.2.1 Channel in UAV Task Offloading and in UAV Energy Harvesting

Equipped with an MEC server, UAV u offers additional computing capacity to nearby UDs. The received signal is given by $V_u = \sum_{d \in \mathcal{D}} h_{d,u} \sqrt{P_d} s_d + n_u$, where s_d satisfies $\mathbb{E}\left\{|s_d|^2\right\} = 1$ and $n_u \sim \mathcal{N}(0, \sigma_u^2)$ is the AWGN. Consequently, the signal-to-noise ratio $\gamma_{d,u}$ and transmission rate $R_{d,u}$ of the UD-to-UAV link can be derived accordingly. Correspondingly, the signal-to-noise ratio $\gamma_{b,u}$ and transmission rate $R_{b,u}$ of the BS-to-UAV link can be derived accordingly.

2.2.2 Channel in BS Task Offloading and in UD Energy Harvesting

Due to its limited onboard energy and the task-accomplishing deadline constraints, UAV u is only capable of executing a portion of the residual tasks it receives, while the remaining part must be relayed to the BS b via the STAR-RIS for further processing. For the STAR-RIS-assisted link, we denote $g_{(m_c,m_r),b}$ as the channel gain from its (m_c, m_r)-th element to the BS. Hence, the composite channel involves two segments: the UD–STAR-RIS link $\boldsymbol{h}_{d,s}$ and the STAR-RIS–BS link $\boldsymbol{g}_{s,b}^H$. The STAR-RIS response to the signal from UD d is modeled by separate coefficient matrices $\boldsymbol{\Theta}_r$ (reflection) and $\boldsymbol{\Theta}_t$ (transmission), each parameterized as $\boldsymbol{\Theta}_a = \mathrm{diag}\left(\sqrt{\beta_{(1,1)}^a} e^{j\theta_{(1,1)}^a}, \ldots, \sqrt{\beta_{(M_c,M_r)}^a} e^{j\theta_{(M_c,M_r)}^a}\right)$. The $\sqrt{\beta_{(m_c,m_r)}^a}$ and $\theta_{(m_c,m_r)}^a$ represent the amplitude and phase shift of element (m_c, m_r) for mode $a \in \{r, t\}$. The ES mode imposes the feasibility condition $\sum_{a \in \{r,t\}} \beta_{(m_c,m_r)}^a \leq 1$.

Accordingly, the composite signal at BS b is obtained as $V_b = \sum_{d \in \mathcal{D}} \boldsymbol{g}_{s,b}^H \boldsymbol{\Theta}_a \boldsymbol{h}_{d,s} \sqrt{P_d} s_d + n_b$, with $n_b = n \sim \mathcal{N}(0, \sigma_b^2)$. Here, $a = t$ if UD d is in the transmission region, and $a = r$ otherwise. Consequently, the SNR $\gamma_{d,b}$ and data rate $R_{d,b}$ for the UD d-to-BS b link are functions of the effective channel gain $\boldsymbol{g}_{s,b}^H \boldsymbol{\Theta}_a \boldsymbol{h}_{d,s}$. Correspondingly, the downlink SNR $\gamma_{b,d}$ and data rate $R_{b,d}$ from BS b to UD d are determined by the effective channel gain $\boldsymbol{g}_{s,d}^H \boldsymbol{\Theta}_a \boldsymbol{h}_{b,s}$ through the STAR-RIS.

Since the achievable rates $R_{i,i'}$ are strongly coupled with the instantaneous SNRs, poor coverage or low-SNR conditions can significantly tighten the energy and latency budgets. Following the insights in Ref. [30], we incorporate adaptive resource allocation via the joint optimization of $\boldsymbol{T}^h$, $\boldsymbol{\alpha}$, and $\boldsymbol{\Theta}$ to mitigate performance degradation under unfavorable channel conditions.

2.3 Energy Harvesting Model

Let T_u^{h} denote the energy harvesting duration of the UAV during the EH phase, T_d^{h} denote the energy harvesting duration of the UDs during the EH phase, and P_b denote the transmit power of the BS, where $0 \le P_b \le P_{b,\max}$ and $P_{b,\max}$ is the maximum allowed transmission power at the BS. Then, the harvested energy of the UAV u during the EH phase can be computed as $E_{b,u}^{\mathrm{h}} = T_u^{\mathrm{h}} \eta P_b h_{b,u}$. $h_{b,u}$ is the channel power gain between the BS b and the UAV u and η $(0 \le \eta \le 1)$ denotes the energy conversion efficiency. Similarly, the harvested energy of the UD d during the EH phase can be computed as $E_{b,d}^{\mathrm{h}}$.

2.4 Task Offloading Model

In this paper, we assume that the computing task is divisible, which means that the task can be divided into more parts. Thus, some computing parts can be first handled locally at the UD, and then some parts can be processed at the UAV u, while the remaining parts can be processed at the BS b. Considering the offloading of task k from UD d, we introduce a continuous decision variable $\alpha_{d,j'}^k \in [0,1]$, where $j' \in \{d, u, b\}$ denotes the candidate execution node (local device, UAV, or BS). This variable represents the fraction of the task k offloaded to node j'. Therefore, the overall offloading strategy is defined by the vector $\boldsymbol{\alpha} = \left\{\alpha_{d,d}^k, \alpha_{d,u}^k, \alpha_{d,b}^k\right\}$, subject to the constraint $\sum_{j' \in \{d,u,b\}} \alpha_{d,j'}^k = 1$.

When task k is uncached, its service latency consists of two components: the uplink transmission time and the remote computation time. In contrast, the downlink delay is ignored because the UAV and BS typically transmit with relatively high power, and the computation results are small in size, making the download time negligible [31]. Specifically, the corresponding energy consumption for offloaded task k from UD d to node j over the uplink is then given by $E_{d,j}^{tr,k} = P_d \frac{\alpha_{d,j}^k L_k}{R_{d,j}}$. Furthermore, the energy consumption for computing the offloaded fraction $\alpha_{d,j'}^k$ of task k at node j' can be expressed as $E_{d,j'}^{com,k} = \kappa_{j'} \frac{\alpha_{d,j'}^k \omega_k}{f_{j'}} f_{j'}^3$, with ω_k, $f_{j'}$, and $\kappa_{j'}$ representing the task's CPU cycle demand, the node's CPU frequency, and its architecture-dependent capacitance coefficient, respectively.

2.5 Caching Model

The content caching strategy is defined by a binary decision variable $X_j^k \in \{0,1\}$, where $X_j^k = 1$ indicates task k is cached at node j, and 0 otherwise. The overall caching strategy is characterized by the vector $\boldsymbol{X} = \left\{X_j^1, X_j^2, \ldots, X_j^k\right\}$. Based on this caching decision, we further characterize the execution delay and energy consumption at the UAV u and the BS b under both cache-hit and cache-miss conditions.

When task k is cached at node $j(X_j^k = 1)$, the corresponding execution delay is denoted by $T_{d,j}^{\mathrm{cache},k}$ and is given by $T_{d,j}^{\mathrm{cache},k} = \frac{\omega_k'}{f_j}$. The ω_k' denotes the CPU cycle count required for the caching operation of task k. Since this computation is performed at the UAV u or the BS b, the major energy consumption is incurred at these nodes, and the energy consumption at the UDs is neglected. Moreover, because the energy required for caching is relatively small compared with that for communication and computation, the UAV is assumed to supply this energy from its onboard battery without relying on the harvested wireless power. Therefore, the energy consumption for caching task k, denoted $E_{d,j}^{\mathrm{cache},k}$, is $E_{d,j}^{\mathrm{cache},k} = \kappa_j \omega_k' f_j^2$. The node j's effective capacitance coefficient κ_j, which depends on the chip architecture of the processor, determines the caching energy consumption.

2.6 Problem Formulation

From the established models of communication, energy harvesting, computation, and caching, we derive the expressions for the total delay T_d^k and energy consumption E_d^k incurred when UD d requests and obtains the result of task k:

$$T_d^k = \sum_{j\in\{u,b\}} X_j^k T_{d,j}^{cache,k} + (1 - \sum_{j\in\{u,b\}} X_j^k) \max\left\{\max\left\{T_u^{\mathrm{h}}, T_d^{\mathrm{h}}\right\} + T_{d,u}^{\mathrm{tr,k}} + T_{d,u}^{\mathrm{com,k}}, T_d^{\mathrm{h}} + T_{d,b}^{\mathrm{tr,k}} + T_{d,b}^{\mathrm{com,k}}, T_d^{\mathrm{h}} + T_{d,d}^{\mathrm{com,k}}\right\}, \tag{1}$$

$$E_d^k = \sum_{j\in\{u,b\}} X_j^k E_{d,j}^{cache,k} + (1 - \sum_{j\in\{u,b\}} X_j^k)(E_{b,u}^{\mathrm{h}} + E_{b,d}^{\mathrm{h}} + E_{d,b}^{com,k}). \tag{2}$$

The total energy consumption consists of three primary components: (i) When the network system caches the task ($X_j^k = 1$), the energy consumption associated with caching the task in the network system is considered; (ii) The energy transmitted to the UAV and UDs through the RF signals sent by the BS; (iii) When the network system does not cache the task ($X_j^k = 0$), the energy consumption is attributed to computation energy consumption of the BS. This paper aims to minimize the total system energy consumption in ASTAR-RIS and WPT-assisted WSNs. This entails the joint optimization of four key variables: the content caching decision $\boldsymbol{X}$, energy harvesting time $\boldsymbol{T}^{\mathrm{h}}$, task offloading decision $\boldsymbol{\alpha}$, and the STAR-RIS resource allocation decision $\boldsymbol{\Theta}$. Accordingly, based on (2), the corresponding total energy minimization problem can be formulated as

$$\mathcal{P}_1: \min_{\boldsymbol{X},\boldsymbol{T}^{\mathrm{h}},\boldsymbol{\alpha},\boldsymbol{\Theta}} \sum_{d\in\mathcal{D}} \sum_{k\in\mathcal{K}} E_d^k \tag{3}$$

$$\text{s.t.} \sum_{d\in\mathcal{D}} E_{d,u}^{com,k} \le E_{b,u}^{\mathrm{h}}, \tag{3a}$$

$$(E_{d,u}^{tr,k} + E_{d,b}^{tr,k} + E_{d,d}^{com,k}) \le E_{b,d}^{\mathrm{h}}, \tag{3b}$$

$$\alpha_{d,j'}^k \in [0,1], \forall d, j' \in \{d,u,b\}, \tag{3c}$$

$$\sum_{j'\in\{d,u,b\}} \alpha_{d,j'}^k = 1, \tag{3d}$$

$$\theta_{(m_c,m_r)}^a \in [0,2\pi), \forall a, \forall m_c, \forall m_r, \tag{3e}$$

$$\sum_{a\in\{r,t\}} \beta_{(m_c,m_r)}^a \le 1, \beta_{(m_c,m_r)}^a \in [0,1], \forall a, \forall m_c, \forall m_r, \tag{3f}$$

$$\sum_{k\in\mathcal{K}} X_j^k S^k \le O_j, \forall k, \forall j, \tag{3g}$$

$$\sum_{k\in\mathcal{K}} \alpha_{d,j'}^k \omega_k \le f_{j'}, \forall k, \forall d, \forall j', \tag{3h}$$

$$\sum_{j\in\{u,b\}} X_j^k \le 1, \forall k, \forall j, \tag{3i}$$

$$X_j^k \in \{0,1\}, \forall k, \forall j, \tag{3j}$$

$$T_d^k \le T_d^{k,\max}, \forall d, \forall k. \tag{3k}$$

Constraints (3a) and (3b) ensure that, at each node, the total energy spent on local computation and task offloading does not exceed the energy harvested during the EH phase. Constraint (3c) restricts the offloading ratio of each node to lie within ([0,1]). Constraint (3d) enforces that, for each task k, the offloading ratios across all possible destinations sum to one. Constraints (3e) and (3f) specify the magnitude and

phase requirements, respectively, for the (m_c, m_r)-th STAR-RIS element applied to the incident signal. The inequality constraint in (3f) follows from the law of energy conservation, which states that the total output power of passive STAR-RIS elements cannot exceed the input power [25]. This formulation is consistent with the general hardware model proposed in [32], where practical insertion losses and design flexibility are accounted for. Constraint (3g) states that each node's total cached content size cannot be greater than its maximum caching capacity. The maximum computing capability of a node cannot be exceeded by the total computing resources used at the node to handle tasks, according to constraint (3h). Constraint (3i) ensures that the same content must not be stored redundantly at both the UAV and BS nodes to achieve cooperative caching. Constraint (3j) restricts the range of all boolean variables to either 0 or 1. Constraint (3k) means that all tasks should be accomplished in the maximum tolerable time.

It is important to note that the energy minimization objective is subject to quality-of-service constraints that ensure system reliability. Specifically, constraint (3k) guarantees task completion within the maximum tolerable delay, while constraints (3a) and (3b) ensure energy sustainability. The STAR-RIS beamforming optimization further enhances transmission reliability by improving effective channel gains. Therefore, the proposed framework achieves energy efficiency without compromising task completion time or data transmission reliability.

In UAV-mounted STAR-RIS systems, mobility may introduce propulsion-energy and endurance trade-offs [33]. In this work, we adopt a quasi-static hovering model during the service period and focus on the WPT-enabled energy-sustainability constraints and the joint optimization of $(\boldsymbol{X}, \boldsymbol{T}^h, \boldsymbol{\alpha}, \boldsymbol{\Theta})$, where WPT further improves the UAV's energy sustainability via RF energy harvesting.

Following the schematic in Fig. 2, problem (3) is addressed by an alternating optimization strategy that partitions it into three subproblems:

- *Caching decision subproblem:* With $\boldsymbol{T}^{\mathrm{h}}$, $\boldsymbol{\alpha}$, and $\boldsymbol{\Theta}$ fixed at their initial values $\boldsymbol{T}^{\mathrm{h}\,0}$, $\boldsymbol{\alpha}^0$, and $\boldsymbol{\Theta}^0$, problem (3) reduces to optimizing the caching decision vector $\boldsymbol{X}$ for total energy minimization, which is addressed using a DRL algorithm to obtain the optimal solution $\boldsymbol{X}^*$.
- *Energy harvesting time subproblem:* With $\boldsymbol{X}$, $\boldsymbol{\alpha}$, and $\boldsymbol{\Theta}$ fixed at $\boldsymbol{X}^*$, $\boldsymbol{\alpha}^0$, and $\boldsymbol{\Theta}^0$, problem (3) reduces to minimizing the total system energy consumption by optimizing the energy harvesting time vector $\boldsymbol{T}^{\mathrm{h}}$, which is solved analytically via the karush-kuhn-tucker (KKT) conditions to obtain the optimal solution $\boldsymbol{T}^{\mathrm{h}\,*}$.
- *Offloading decision subproblem:* With $\boldsymbol{X}$, $\boldsymbol{T}^{\mathrm{h}}$, and $\boldsymbol{\Theta}$ fixed at $\boldsymbol{X}^*$, $\boldsymbol{T}^{\mathrm{h}\,*}$, and $\boldsymbol{\Theta}^0$, problem (3) reduces to minimizing the total system energy consumption over the offloading decision vector $\boldsymbol{\alpha}$, which is solved via the KKT conditions to yield the optimal solution $\boldsymbol{\alpha}^*$.
- *STAR-RIS resource allocation subproblem:* With $\boldsymbol{X}$, $\boldsymbol{T}^{\mathrm{h}}$, and $\boldsymbol{\alpha}$ fixed at their optimal values $\boldsymbol{X}^*$, $\boldsymbol{T}^{\mathrm{h}\,*}$, and $\boldsymbol{\alpha}^*$, the problem reduces to minimizing the total system energy consumption over the STAR-RIS resource allocation decision $\boldsymbol{\Theta}$, which is solved via the SCA method to obtain the optimal solution $\boldsymbol{\Theta}^*$.

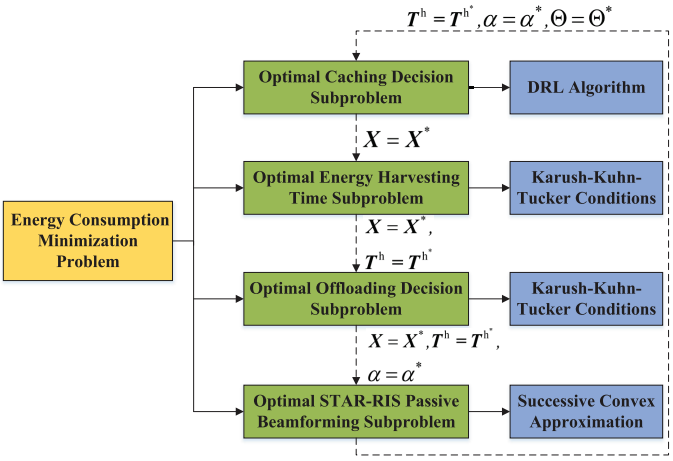

Figure 2: The joint optimization scheme for minimizing the total energy consumption.

3 Content Caching Decision Optimization

Due to its dependence only on $\boldsymbol{X}$ and not on other variables in $\mathcal{P}_1$, the caching decision optimization can be addressed beforehand once the energy harvesting time, offloading decisions, and passive beamforming are fixed. This leads to the following subproblem formulation:

$$\mathcal{P}_2: \min_{\boldsymbol{X}} \sum_{d\in\mathcal{D}} \sum_{k\in\mathcal{K}} E_d^k \tag{4}$$
$$\text{s.t. } (3g)-(3k)$$

Since $\boldsymbol{X}$ is a continuous probability vector, $\mathcal{P}_2$ belongs to a continuous nonlinear programming problem. Caching decision optimization is a dynamically adjusted optimization problem rather than a static convex optimization problem. Owing to the highly non-convex and coupled structure of the problem, conventional optimization methods are prone to getting trapped in local optima rather than locating the global optimum. To overcome this limitation, we employ the twin delayed deep deterministic policy gradient (TD3) algorithm, a representative state-of-the-art DRL approach, to tackle the caching decision subproblem. TD3 is capable of handling continuous probability vectors and is designed to learn optimal caching policies in complex environments. In this context, the entire caching system is modeled as an agent that interacts with the environment. This interaction enables the agent to approximate an optimal caching policy over time. To achieve better optimization performance, we design the state space, action space, and reward function in the proposed intelligent caching markov decision process (MDP) model as follows:

- **State:** At time slot (t), the agent state is defined as $s_t = \{\mathcal{P}_t, \mathcal{Q}_t, \mathcal{C}_t, \mathcal{E}_t, \mathcal{O}_t\}$. $\mathcal{P}_t$ denotes the content popularity, modeled by a time-varying zipf distribution; $\mathcal{Q}_t = [\mathcal{Q}_{1,t}, \mathcal{Q}_{2,t}, \ldots, \mathcal{Q}_{K,t}]$ captures the historical request frequency; $\mathcal{C}_t = [\mathcal{C}_{u,t}, \mathcal{C}_{c,t}]$ describes the caching status at the UAV and the BS; $\mathcal{E}_t = [\mathcal{E}_{d_1,t}, \mathcal{E}_{d_2,t}, \ldots, \mathcal{E}_{D,t}, \mathcal{E}_{u,t}]$ characterizes the energy harvesting status of all UDs and the UAV; The term $\mathcal{O}_t$ represents the relevant network topology information at slot t.
- **Action:** In the caching decision stage, the continuous action a_t encodes the caching probabilities at both the UAV and the BS, $a_t = \left[\pi^u_{1,t+1}, \ldots, \pi^u_{K,t+1}, \pi^b_{1,t+1}, \ldots, \pi^b_{K,t+1}\right]$. The $\pi^u_{k,t+1}$ and $\pi^b_{k,t+1}$ represent the probabilities of placing content k in the UAV cache and BS cache, respectively. Then select top-K_{UAV} and top-K_{BS} contents respectively based on probabilities.
- **Reward:** The reward function is a key component for steering the agent's exploration in the caching update task and for ensuring stable convergence. Accordingly, at time slot t, we define

$r_t = \lambda_1 \sum_{j\in\{u,c\}} \mathcal{A}_t^j - \lambda_2 W_t$. The λ_1 and λ_2 are the weight parameters used to balance different optimization objectives; The variable $\mathcal{A}_t^j$ captures the cache-hit count at node j (UAV or BS) during slot t, serving as a direct metric for caching efficiency; and W_t denotes the number of cache switching operations, which incurs energy consumption of storage overhead and computational cost, thus requiring minimization.

The TD3-based caching policy dynamically adapts to varying task types and urgency through the comprehensive state representation. The content popularity $\mathcal{P}_t$ and historical request frequency $\mathcal{Q}_t$ enable the agent to learn temporal patterns and prioritize time-sensitive or frequently requested content. The energy harvesting status $\mathcal{E}_t$ further allows the policy to balance caching benefits against energy constraints. During each decision epoch, the agent evaluates the current state and outputs caching probabilities that reflect the expected value of caching each content type, thereby achieving dynamic adaptation to heterogeneous task characteristics.

4 Energy Harvesting Time, Offloading Decision, and STAR-RIS Resource Allocation

After the caching policy is obtained by the TD3-based module, the energy harvesting time $\boldsymbol{T}^{\mathrm{h}}$, task offloading vector $\boldsymbol{\alpha}$, and STAR-RIS resource allocation decision $\boldsymbol{\Theta}$ are further refined through an iterative procedure that combines the KKT conditions with SCA. Accordingly, problem (3) can be reformulated as

$$\mathcal{P}_3: \min_{\boldsymbol{T}^{\mathrm{h}},\boldsymbol{\alpha},\boldsymbol{\Theta}} \sum_{d\in\mathcal{D}}\sum_{k\in\mathcal{K}} \left(\sum_{j\in\{u,b\}} X_j^{k*} E_{d,j}^{cache,k} + \left(1 - \sum_{j\in\{u,b\}} X_j^{k*}\right)\left(E_{b,u}^{\mathrm{h}} + E_{b,d}^{\mathrm{h}} + E_{d,b}^{com,k}\right)\right)$$

s.t. (3a)–(3f), (3h), (3k),

$$\sum_{k\in\mathcal{K}} X_j^{k*} S^k \le O_j, \quad \forall k, \forall j, \tag{5a}$$

$$X_j^{k*} \in \{0,1\}, \quad \forall k, \forall j, \tag{5b}$$

$$\sum_{j\in\{u,b\}} X_j^{k*} \le 1, \forall k, \forall j. \tag{5c}$$

4.1 Energy Harvesting Time

Given that the content caching strategy $\boldsymbol{X} = \boldsymbol{X}^*$, offloading decision $\boldsymbol{\alpha} = \boldsymbol{\alpha}^0$, and STAR-RIS resource allocation $\boldsymbol{\Theta} = \boldsymbol{\Theta}^0$ are fixed, the energy harvesting time $\boldsymbol{T}^{\mathrm{h}} = \left\{T_u^{\mathrm{h}}, T_d^{\mathrm{h}}\right\}$ optimization problem is formulated to minimize the total energy consumption. The problem (5) is rewritten as:

$$\min_{T_u^{\mathrm{h}}, T_d^{\mathrm{h}}} \quad \sum_{d\in\mathcal{D}}\sum_{k\in\mathcal{K}} \left(T_u^{\mathrm{h}} \eta P_b h_{b,u}^0 + T_d^{\mathrm{h}} \eta P_b h_{b,d}^0\right) \tag{6a}$$

$$\text{s.t.} \quad \sum_{d\in\mathcal{D}} E_{d,u}^{com,k} \le T_u^{\mathrm{h}} \eta P_b h_{b,u}^0, \forall d, \forall k, \tag{6b}$$

$$E_{d,u}^{tr,k} + E_{d,b}^{tr,k} + E_{d,d}^{com,k} \le T_d^{\mathrm{h}} \eta P_b h_{b,d}^0, \forall d, \forall k, \tag{6c}$$

$$T_d^k \le T_d^{k,\max}, \forall d, \forall k, \tag{6d}$$

where $h_{b,d}^0$ is determined by the given STAR-RIS parameters $\boldsymbol{\Theta}^0$. The corresponding lagrangian of problem (7), denoted by $L\left(T_u^{\mathrm{h}}, T_d^{\mathrm{h}}, \boldsymbol{\lambda}, \boldsymbol{\nu}, \boldsymbol{\xi}\right)$, can be expressed as:

$$\begin{aligned}\mathcal{L} = \sum_{d\in\mathcal{D}}\sum_{k\in\mathcal{K}}\Bigg(& T_u^{\mathrm{h}}\eta P_b h_{b,u}^0 + T_d^{\mathrm{h}}\eta P_b h_{b,d}^0 + \lambda_{d,k}\left(\sum_{d\in\mathcal{D}} E_{d,u}^{\mathrm{com},k} - T_u^{\mathrm{h}}\eta P_b h_{b,u}\right) \\ &+ \nu_{d,k}\left(E_{d,u}^{\mathrm{tr},k} + E_{d,b}^{\mathrm{tr},k} + E_{d,d}^{\mathrm{com},k} - T_d^{\mathrm{h}}\eta P_b h_{b,d}^0\right) + \xi_{d,k}\left(T_d^k - T_d^{k,\max}\right)\Bigg).\end{aligned} \tag{7}$$

The optimal energy harvesting time vector $T^{h*} = \left(T_u^{h*}, T_d^{h*}\right)$ can be derived from the KKT conditions as follows:

$$T^{h*} = \underset{\{\tilde{T}_u^h, \tilde{T}_d^h, \tilde{\boldsymbol{\lambda}}, \tilde{\boldsymbol{\nu}}, \tilde{\boldsymbol{\xi}}\}}{\arg\min}\ E_{\mathrm{EH}}^{\mathrm{total}}\left(\boldsymbol{X}^*, T_u^h, T_d^h, \boldsymbol{\alpha}^0, \boldsymbol{\Theta}^0\right). \tag{8}$$

The feasible solution set $\mathcal{M}_{\mathrm{EH}}$ can be derived by solving the KKT conditions (9). Any point $\left\{\tilde{T}_u^{\mathrm{h}}, \tilde{T}_d^{\mathrm{h}}, \tilde{\boldsymbol{\lambda}}, \tilde{\boldsymbol{\nu}}, \tilde{\boldsymbol{\xi}}\right\}$ satisfying these conditions belongs to $\mathcal{M}_{\mathrm{EH}}$, and the optimal energy harvesting times correspond to the solution presented in (8).

$$\left.\frac{\partial L}{\partial T_u^{\mathrm{h}}}\right|_{T_u^{\mathrm{h}}=\tilde{T}_u^{\mathrm{h}}, \boldsymbol{\lambda}=\tilde{\boldsymbol{\lambda}}, \boldsymbol{\nu}=\tilde{\boldsymbol{\nu}}, \boldsymbol{\xi}=\tilde{\boldsymbol{\xi}}} = 0, \tag{9a}$$

$$\left.\frac{\partial L}{\partial T_d^{\mathrm{h}}}\right|_{T_d^{\mathrm{h}}=\tilde{T}_d^{\mathrm{h}}, \boldsymbol{\lambda}=\tilde{\boldsymbol{\lambda}}, \boldsymbol{\nu}=\tilde{\boldsymbol{\nu}}, \boldsymbol{\xi}=\tilde{\boldsymbol{\xi}}} = 0, \tag{9b}$$

$$\sum_{d\in\mathcal{D}} E_{d,u}^{com,k} \le T_u^{\mathrm{h}}\eta P_b h_{b,u}^0, \forall d, \forall k, \tag{9c}$$

$$E_{d,u}^{tr,k} + E_{d,b}^{tr,k} + E_{d,d}^{com,k} \le T_d^{\mathrm{h}}\eta P_b h_{b,d}^0, \forall d, \forall k, \tag{9d}$$

$$T_d^k \le T_d^{k,\max}, \forall d, \forall k, \tag{9e}$$

$$\tilde{\lambda}_{d,k}\left(\sum_{d\in\mathcal{D}} E_{d,u}^{com,k} - T_u^{\mathrm{h}}\eta P_b h_{b,u}\right) = 0, \forall d, \forall k, \tag{9f}$$

$$\tilde{\nu}_{d,k}\left(E_{d,u}^{tr,k} + E_{d,b}^{tr,k} + E_{d,d}^{com,k} - T_d^{\mathrm{h}}\eta P_b h_{b,d}^0\right) = 0, \forall d, \forall k, \tag{9g}$$

$$\tilde{\xi}_{d,k}\left(T_d^k - T_d^{k,\max}\right) = 0, \forall d, \forall k, \tag{9h}$$

$$\tilde{\lambda}_{d,k} \ge 0, \tilde{\nu}_{d,k} \ge 0, \forall d, \tilde{\xi}_{d,k} \ge 0, \forall k. \tag{9i}$$

4.2 Offloading Decision

Given that the caching decision $\boldsymbol{X} = \boldsymbol{X}^*$, energy harvesting time $\boldsymbol{T}^{\mathrm{h}} = \boldsymbol{T}^{\mathrm{h}*}$, and STAR-RIS resource allocation $\boldsymbol{\Theta} = \boldsymbol{\Theta}^0$ are fixed, the offloading decision $\boldsymbol{\alpha}$ optimization problem aims to minimize the total energy consumption. The problem (5) is reformulated as:

$$\min_{\boldsymbol{\alpha}}\quad \sum_{d\in\mathcal{D}}\sum_{k\in\mathcal{K}}\left(\left(1 - \sum_{j\in\{u,b\}} X_j^{k^*}\right)\kappa_b \alpha_{d,b}^k \omega_k f_b^2\right) \tag{10a}$$

$$\text{s.t.}\quad \text{(3a)}-\text{(3d)}, \text{(3h)}, \text{(3k)}.$$

The Lagrange function is constructed as:

$$\begin{aligned}\mathcal{L} = \sum_{d\in\mathcal{D}}\sum_{k\in\mathcal{K}}\Bigg(&\left(\left(1-\sum_{j\in\{u,b\}} X_j^{k\,*}\right)\kappa_b\alpha_{d,b}^k\omega_k f_b^2 + \eta_{d,k}\left(\sum_{d\in\mathcal{D}} E_{d,u}^{com,k} - E_{b,u}^{\mathrm{h}}\right) + \sum_{j'\in\{d,u,b\}}\varepsilon_{d,k}^1\left(\alpha_{d,j'}^k - 1\right)\right.\\ &+ \mu_{d,k}\left(E_{d,u}^{tr,k} + E_{d,b}^{tr,k} + E_{d,d}^{com,k} - E_{b,d}^{\mathrm{h}}\right) + \sum_{j'\in\{d,u,b\}}\varepsilon_{d,k}^2\left(-\alpha_{d,j'}^k\right) + \chi_{d,k}\left(\sum_{j'\in\{d,u,b\}}\alpha_{d,j'}^k - 1\right)\\ &\left.+ \zeta_{d,k}\left(\sum_{k\in\mathcal{K}}\alpha_{d,j'}^k\omega_k - f_{j'}\right) + \xi_{d,k}\left(T_d^k - T_d^{k,\max}\right)\right)\end{aligned} \tag{11}$$

The optimal offloading vector $\boldsymbol{\alpha}^*$, obtained via the KKT conditions, can be expressed as:

$$\boldsymbol{\alpha}^* = \underset{\{\tilde{\boldsymbol{\alpha}},\tilde{\boldsymbol{\eta}},\tilde{\boldsymbol{\mu}},\tilde{\boldsymbol{\varepsilon}}^1,\tilde{\boldsymbol{\varepsilon}}^2,\tilde{\boldsymbol{\chi}},\tilde{\boldsymbol{\zeta}},\tilde{\boldsymbol{\xi}}\}}{\arg\min}\; E_{\mathrm{OFF}}^{\mathrm{total}}\left(\boldsymbol{X}^*, \boldsymbol{T}^{\mathrm{h}\,*}, \boldsymbol{\alpha}, \boldsymbol{\Theta}^0\right). \tag{12}$$

Any point $\{\tilde{\boldsymbol{\alpha}}, \tilde{\boldsymbol{\eta}}, \tilde{\boldsymbol{\mu}}, \tilde{\boldsymbol{\varepsilon}}^1, \tilde{\boldsymbol{\varepsilon}}^2, \tilde{\boldsymbol{\chi}}, \tilde{\boldsymbol{\zeta}}, \tilde{\boldsymbol{\xi}}\}$ that satisfies the KKT conditions (13) lies within the feasible set $\mathcal{M}_{\mathrm{OFF}}$. Consequently, solving (13) allows $\mathcal{M}_{\mathrm{OFF}}$ to be derived, and the optimal offloading decision given in (12) to be obtained.

$$\left.\frac{\partial\mathcal{L}}{\partial\alpha_{d,j'}^k}\right|_{\alpha_{d,j'}^k=\tilde{\alpha}_{d,j'}^k,\boldsymbol{\eta}=\tilde{\boldsymbol{\eta}},\boldsymbol{\mu}=\tilde{\boldsymbol{\mu}},\boldsymbol{\varepsilon}^1=\tilde{\boldsymbol{\varepsilon}}^1,\boldsymbol{\varepsilon}^2=\tilde{\boldsymbol{\varepsilon}}^2,\boldsymbol{\chi}=\tilde{\boldsymbol{\chi}},\boldsymbol{\zeta}=\tilde{\boldsymbol{\zeta}},\boldsymbol{\xi}=\tilde{\boldsymbol{\xi}}} = 0, \tag{13a}$$

(3a)–(3d), (3h), (3k),

$$\tilde{\eta}_{d,k}\left(\sum_{d\in\mathcal{D}} E_{d,u}^{com,k} - E_{b,u}^{\mathrm{h}}\right) = 0, \quad \forall d, \forall k, \tag{13b}$$

$$\tilde{\mu}_{d,k}\left(E_{d,u}^{tr,k} + E_{d,b}^{tr,k} + E_{d,d}^{com,k} - E_{b,d}^{\mathrm{h}}\right) = 0, \quad \forall d, \forall k, \tag{13c}$$

$$\tilde{\varepsilon}_{d,k}^1\left(\alpha_{d,j'}^k - 1\right) = 0, \quad \forall d, \forall j', \forall k, \tag{13d}$$

$$\tilde{\varepsilon}_{d,k}^2\alpha_{d,j'}^k = 0, \quad \forall d, \forall j', \forall k, \tag{13e}$$

$$\tilde{\chi}_{d,k}\left(\sum_{j'\in\{d,u,b\}}\alpha_{d,j'}^k - 1\right) = 0, \quad \forall d, \forall j', \forall k, \tag{13f}$$

$$\tilde{\zeta}_{d,k}\left(\sum_{k\in\mathcal{K}}\alpha_{d,j'}^k\omega_k - f_{j'}\right) = 0, \quad \forall d, \forall j', \forall k, \tag{13g}$$

$$\tilde{\xi}_{d,k}\left(T_d^k - T_d^{k,\max}\right) = 0, \quad \forall d, \forall j', \forall k, \tag{13h}$$

$$\tilde{\eta}_{d,k} \geq 0, \tilde{\mu}_{d,k} \geq 0, \tilde{\varepsilon}_{d,k}^1 \geq 0, \tilde{\varepsilon}_{d,k}^2 \geq 0, \tilde{\zeta}_{d,k} \geq 0, \tilde{\xi}_{d,k} \geq 0, \quad \forall d, \forall k, \tag{13i}$$

where $\tilde{\chi}_{d,k}$ is a Lagrange multiplier associated with an equality constraint and is treated as an unrestricted multiplier consistent.

4.3 STAR-RIS Passive Beamforming

Given $\boldsymbol{X} = \boldsymbol{X}^*$, $\boldsymbol{T}^{\mathrm{h}} = \boldsymbol{T}^{\mathrm{h}\,*}$, and $\boldsymbol{\alpha} = \boldsymbol{\alpha}^*$, problem (5) is reformulated as:

$$\min_{\boldsymbol{\Theta}} \quad \sum_{d\in\mathcal{D}}\sum_{k\in\mathcal{K}}\left(T_d^{\mathrm{h}}\eta P_b\left|\boldsymbol{g}_{s,d}^H\boldsymbol{\Theta}_a\boldsymbol{h}_{b,s}\right|\right) \tag{14a}$$

$$\text{s.t.} \quad \text{(3b), (3e), (3f), (3k).}$$

In order to deal with the non-convex problem, the SCA method is adopted. First, define the auxiliary variable $\zeta_{d,k} \geq 0$, satisfying: $\zeta_{d,k} \geq \left|\boldsymbol{g}_{s,d}^H \boldsymbol{\Theta}_a \boldsymbol{h}_{b,s}\right|$. Second, we convert the quadratic term $\left|\boldsymbol{g}_{s,d}^H \boldsymbol{\Theta}_a \boldsymbol{h}_{b,s}\right|^2$ as $\left|\boldsymbol{v}_a^H \mathbf{y}\right|^2$, where $\mathbf{y} = \text{diag}(\boldsymbol{g}_{s,d}^H)\boldsymbol{h}_{b,s}$. Then we apply first-order taylor expansion to the quadratic term $\zeta_{d,k}^2$ and update the linearization point in each iteration. Specifically, the result $\zeta_{d,k}^{[t-1]}$ from the previous iteration is employed as the current reference $\zeta_{d,k}^{[t]}$. $(\zeta_{d,k}^{[t]})^2 + 2\zeta_{d,k}^{[t]}(\zeta_{d,k} - \zeta_{d,k}^{[t]}) \geq \boldsymbol{v}_a^H \mathbf{y}\mathbf{y}^H \boldsymbol{v}_a$. $\boldsymbol{v}_a = \text{vec}(\boldsymbol{\Theta}_a)$, and $\zeta_{d,k}^{[t]}$ denote the value at the tth iteration. Consequently, constraints (3f) and (3g) are reformulated as the following convex constraint:

$$\sum_{a\in\{r,t\}} \boldsymbol{v}_a^2\left[(m_c, m_r)\right] \leq 1, \tag{15}$$

where $\boldsymbol{v}_a\left[(m_c, m_r)\right]$ is the (m_c, m_r)-th element of $\boldsymbol{v}_a^H$. Since it is a quadratic function and the feasible set is convex, this constraint (15) is strictly convex, thereby ensuring the validity of the convex reformulation. Therefore, the convexified problem is written as:

$$\min_{\boldsymbol{v}_a, \boldsymbol{\zeta}} \quad \sum_{d\in\mathcal{D}} \sum_{k\in\mathcal{K}} T_d^{\text{h}} \eta P_b \zeta_{d,k} \tag{16a}$$

$$\text{s.t.} \quad \boldsymbol{v}_a^H \mathbf{y}\mathbf{y}^H \boldsymbol{v}_a \leq (\zeta_{d,k}^{[t]})^2 + 2\zeta_{d,k}^{[t]}(\zeta_{d,k} - \zeta_{d,k}^{[t]}), \ \forall d, k \tag{16b}$$

(15), (3b), (3k).

The lagrangian function L is defined as follows:

$$\begin{aligned} L(\boldsymbol{v}_a, \boldsymbol{\zeta}, \boldsymbol{\gamma}, \boldsymbol{\lambda}, \boldsymbol{\mu}, \boldsymbol{\xi}) = \sum_{d\in\mathcal{D}} \sum_{k\in\mathcal{K}} \Bigg(& T_d^{\text{h}} \eta P_b \zeta_{d,k} + \lambda_{d,k} \left(\boldsymbol{v}_a^H \mathbf{y}\mathbf{y}^H \boldsymbol{v}_a - (\zeta_{d,k}^{[t]})^2 - 2\zeta_{d,k}^{[t]}(\zeta_{d,k} - \zeta_{d,k}^{[t]}) \right) \\ & + \gamma_{d,k} \left(E_{d,u}^{tr,k} + E_{d,b}^{tr,k} + E_{d,d}^{com,k} - E_{b,d}^{\text{h}} \right) + \mu_{d,k} \left(\sum_{a\in\{r,t\}} \boldsymbol{v}_a^2\left[(m_c, m_r)\right] - 1 \right) + \xi_{d,k} \left(T_d^k - T_d^{k,\max} \right) \Bigg), \end{aligned} \tag{17}$$

where $\boldsymbol{\gamma}$, $\boldsymbol{\lambda}$, $\boldsymbol{\mu}$, and $\boldsymbol{\xi}$ are the lagrangian multipliers associated with the four constraints of problem (16). The lagrangian dual function is written as $D(\boldsymbol{\gamma}, \boldsymbol{\lambda}, \boldsymbol{\mu}, \boldsymbol{\xi}) = \min_{\boldsymbol{v}_a, \boldsymbol{\zeta}} L(\boldsymbol{v}_a, \boldsymbol{\zeta}, \boldsymbol{\gamma}, \boldsymbol{\lambda}, \boldsymbol{\mu}, \boldsymbol{\xi})$. The KKT conditions must be satisfied at optimality for both problem (16) and its dual $(D(\boldsymbol{\gamma}, \boldsymbol{\lambda}, \boldsymbol{\mu}, \boldsymbol{\xi}))$, by virtue of the convexity of the primal problem. By setting $\frac{\partial L}{\partial \boldsymbol{v}_a} = 0$ and $\frac{\partial L}{\partial \boldsymbol{\zeta}} = 0$ and solving the resulting equations, the optimal solution $\boldsymbol{v}_a^*$ and $\boldsymbol{\zeta}^*$ are derived as $\boldsymbol{v}_a^* = \arg\min_{\boldsymbol{v}_a} L(\boldsymbol{v}_a, \boldsymbol{\zeta}, \boldsymbol{\gamma}, \boldsymbol{\lambda}, \boldsymbol{\mu}, \boldsymbol{\xi})$ and $\boldsymbol{\zeta}^* = \arg\min_{\boldsymbol{\zeta}} L(\boldsymbol{v}_a, \boldsymbol{\zeta}, \boldsymbol{\gamma}, \boldsymbol{\lambda}, \boldsymbol{\mu}, \boldsymbol{\xi})$. The lagrangian multipliers $\boldsymbol{\gamma}$, $\boldsymbol{\lambda}$, $\boldsymbol{\mu}$, $\boldsymbol{\xi}$ are updated according to:

$$\gamma^{[k+1]} = \left[\gamma^{[k]} + \Delta_\gamma[k] \left(E_{d,u}^{tr,k} + E_{d,b}^{tr,k} + E_{d,d}^{com,k} - E_{b,d}^{\text{h}} \right) \right]^+; \tag{18}$$

$$\lambda^{[k+1]} = \left[\lambda^{[k]} + \Delta_\lambda[k] \left(\boldsymbol{v}_a^H \mathbf{y}\mathbf{y}^H \boldsymbol{v}_a - (\zeta_{d,k}^{[t]})^2 - 2\zeta_{d,k}^{[t]}(\zeta_{d,k} - \zeta_{d,k}^{[t]}) \right) \right]^+; \tag{19}$$

$$\mu^{[k+1]} = \left[\mu^{[k]} + \Delta_\mu[k] \left(\sum_{a\in\{r,t\}} \boldsymbol{v}_a^2\left[(m_c, m_r)\right] - 1 \right) \right]^+; \tag{20}$$

$$\xi^{[k+1]} = \left[\xi^{[k]} + \Delta_\xi[k] \left(T_d^k - T_d^{k,\max} \right) \right]^+; \tag{21}$$

The step size vector $\boldsymbol{\Delta}_2[k] = (\Delta_\gamma[k], \Delta_\lambda[k], \Delta_\mu[k], \Delta_\xi[k])^T$ updates the lagrangian multipliers $\boldsymbol{\gamma}$, $\boldsymbol{\lambda}$, $\boldsymbol{\mu}$, and $\boldsymbol{\xi}$ in the k-th iteration, and is refreshed in each subsequent iteration. The non-negativity of multipliers is preserved by the projection operator $[\cdot]^+ = \max(\cdot, 0)$.

Given the optimal variables $\boldsymbol{v}_a^*$ and $\boldsymbol{\zeta}^*$, the corresponding optimal STAR-RIS resource allocation decision is constructed as $\boldsymbol{\Theta}_a^* = \mathrm{diag}(\boldsymbol{v}_a^*)^H$. $\boldsymbol{v}_a^*$ is iteratively updated to ensure convergence to a stable point that satisfies all constraints.

5 Convergence and Complexity Analysis of DRL-SCA Algorithm

Algorithm 1 presents the workflow of the DRL–SCA framework, in which the caching decision is first obtained by the DRL module and then used as a fixed parameter to iteratively optimize the energy harvesting time, offloading decision, and STAR-RIS resource allocation decision. In what follows, we investigate the algorithm's convergence and demonstrate that it can reach a locally suboptimal point within a finite number of processes. At last, computational complexity analysis.

Algorithm 1: DRL-SCA-based content caching decision, energy harvesting time, task offloading decision, and STAR-RIS resource allocation decision for WSNs

1 Initializations: the energy harvesting time $\boldsymbol{T}^{\mathrm{h}^0}$, task offloading decision $\boldsymbol{\alpha}^0$, and STAR-RIS resource allocation decision $\boldsymbol{\Theta}^0$, and set iteration index $v = 0$

2 repeat

3 Given $\{\boldsymbol{T}^{\mathrm{h}^v}, \boldsymbol{\alpha}^v, \boldsymbol{\Theta}^v\}$, solve (4) and the feasible solution $\boldsymbol{X}^{v+1}$ can be obtained by $a_t = \mathrm{Sample}(\pi_\theta(\cdot \mid s_t))$, where π_θ is obtained according to TD3-based caching decision process;

4 With $\{\boldsymbol{X}^{v+1}, \boldsymbol{T}^{\mathrm{h}^v}, \boldsymbol{\alpha}^v, \boldsymbol{\Theta}^v\}$ fixed, solve (6) by CVX and obtain the updated energy harvesting time $\boldsymbol{T}^{\mathrm{h}^{v+1}}$;

5 With $\{\boldsymbol{X}^{v+1}, \boldsymbol{T}^{\mathrm{h}^{v+1}}, \boldsymbol{\alpha}^v, \boldsymbol{\Theta}^v\}$ fixed, solve (10) by CVX and obtain the updated task offloading decision $\boldsymbol{\alpha}^{v+1}$;

6 With $\{\boldsymbol{X}^{v+1}, \boldsymbol{T}^{\mathrm{h}^{v+1}}, \boldsymbol{\alpha}^{v+1}, \boldsymbol{\Theta}^v\}$ fixed, solve (14) by CVX and obtain the updated STAR-RIS resource allocation decision $\boldsymbol{\Theta}^{v+1}$;

7 $v \leftarrow v + 1$;

8 until *The relative improvement of the objective value falls below a predefined threshold;*

Output: $\boldsymbol{X}^*$, $\boldsymbol{T}^{\mathrm{h}^*}$, $\boldsymbol{\alpha}^*$, $\boldsymbol{\Theta}^*$.

5.1 Convergence Analysis

Lemma 1: *Algorithm 1 generates a non-increasing objective sequence and converges to a stationary solution under the prescribed stopping criterion.*

Proof: Let $E^{(v)}$ denote the objective value at the v-th outer iteration. The proposed algorithm follows a block coordinate descent (BCD) structure over $\boldsymbol{X}$, $\boldsymbol{T}^{\mathrm{h}}$, $\boldsymbol{\alpha}$, $\boldsymbol{\Theta}$.

Descent property of block updates: For fixed $\boldsymbol{X}$, the EH-time and offloading subproblems are convex and are solved optimally, hence they do not increase the objective. For the STAR-RIS block, the SCA procedure solves a sequence of convexified subproblems that provide upper bounds on the original non-convex objective at the current iterate, which ensures a non-increasing objective across SCA iterations and thus across outer iterations. For the caching block, the TD3 agent is trained offline to yield a stable policy. In the online procedure, the caching decision $\boldsymbol{X}^{v+1}$ is obtained by policy inference and then projected onto the feasible binary set under cache-size constraints. To ensure monotonicity in the outer loop, we apply

an acceptance check: if the updated caching decision does not decrease the objective, we keep $\boldsymbol{X}^{v+1} = \boldsymbol{X}^{v}$. Therefore, the overall objective sequence satisfies $E^{(v+1)} \leq E^{(v)}$.

Lower boundedness: Since $E^{(v)}$ represents total system energy consumption, it is non-negative, i.e., $E^{(v)} \geq 0$.

Convergence: Because $E^{(v)}$ is non-increasing and lower bounded, it converges. Upon termination (when the relative improvement falls below a threshold), the algorithm reaches a stationary point of the BCD procedure. □

The above result demonstrates that the original problem $\mathcal{P}_1$ is decomposed into four subproblems and solved iteratively via block coordinate descent (BCD). At every iteration, the obtained solution serves as the starting point for the next one. Each block-wise update, encompassing caching decision optimization via DRL, energy harvesting time optimization, offloading decision optimization, and STAR-RIS resource allocation decision optimization, yields a non-increasing overall objective. Consequently, convergence to a stationary point (local suboptimum) is guaranteed, provided that the algorithm is terminated once the objective improvement becomes negligible or a maximum iteration limit is reached.

5.2 Computational Complexity Analysis

The complexity is analyzed by separating the offline TD3 training stage and the online alternating optimization stage.

Offline TD3 training: The TD3 caching agent is trained offline. The total training complexity is $\mathcal{O}(N_{\text{epi}} \cdot N_{\text{step}} \cdot (C_{\text{actor}} + C_{\text{critic}}))$, where N_{epi} and N_{step} denote the number of training episodes and steps per episode, and C_{actor}, C_{critic} denote the computational cost of one forward/backward update of the actor/critic networks.

Online alternating optimization: At runtime, TD3 only performs policy inference (a forward pass) with complexity $\mathcal{O}(C_{\text{actor}})$, followed by a feasible projection to obtain binary caching decisions. The EH-time and offloading subproblems are convex and can be solved by interior-point methods with complexity on the order of $\mathcal{O}(n^3 \log(1/\varepsilon))$, where n denotes the number of decision variables and ε is the solver accuracy. The STAR-RIS block uses SCA with N_{SCA} inner iterations; each iteration solves a convexified problem whose dimension scales with the number of STAR-RIS elements $M = M_c M_r$, yielding complexity $\mathcal{O}(N_{\text{SCA}} \cdot n_{\Theta}^3 \log(1/\varepsilon))$ with $n_{\Theta} = \mathcal{O}(M)$.

The $n_{\text{EH}} = \mathcal{O}(D)$, $n_{\alpha} = \mathcal{O}(DK)$, and $n_{\Theta} = \mathcal{O}(M_c M_r)$ represent the number of decision variables in the EH-time, offloading, and STAR-RIS subproblems, respectively, where D is the number of UDs and K is the number of tasks. Let N_{iter} be the number of outer iterations. So, the overall online complexity is $\mathcal{O}\left(N_{\text{iter}}\left(C_{\text{actor}} + n_{\text{EH}}^3 \log\frac{1}{\varepsilon} + n_{\alpha}^3 \log\frac{1}{\varepsilon} + N_{\text{SCA}} \cdot n_{\Theta}^3 \log\frac{1}{\varepsilon}\right)\right)$.

6 Performance Evaluation and Discussion

To assess the effectiveness of the proposed energy-efficient ASTAR-RIS and WPT-assisted task offloading and content caching framework for WSNs, we consider the following simulation setup. The UAV u, the ground BS b, and the STAR-RIS are placed at $(0, 0, 20)$ m, $(0, 40, 0)$ m, and $(0, 0, 20)$ m, respectively. Four ground UDs are located at $(-40, -40, 0)$ m, $(-40, 40, 0)$ m, $(40, -40, 0)$ m, and $(40, 40, 0)$ m, forming a representative distributed sensor network layout [34].

The UAV is positioned at $(0, 0, 20)$ m, which is the geometric center of the considered symmetric UD topology. This placement yields balanced large-scale path loss to the UDs and avoids favoring any particular user, thereby serving as a controlled baseline to evaluate the energy-efficiency gains brought by the proposed WPT-assisted ASTAR-RIS joint optimization. We emphasize that the purpose of fixing the hovering location is to isolate the benefits of WPT integration and joint resource optimization; varying the

hovering point would affect the absolute energy values but not the qualitative insights or the role of each optimized component.

Furthermore, to highlight the benefits of the proposed framework, we benchmark it against several representative baseline schemes, namely no STAR-RIS, no energy harvesting (no EH), no caching, full offloading [35,36]. These baselines enable us to quantitatively assess the contribution of joint optimization of caching, energy harvesting, offloading, and STAR-RIS configuration to energy savings and system performance enhancement. The configurations of some simulation schemes are specified as follows.

- *Proposed:* In the ASTAR-RIS and WPT-assisted WSNs, the total energy consumption is reduced by performing a joint optimization over content caching decisions, energy harvesting time, task offloading decisions, and STAR-RIS resource allocation decisions.
- *No EH:* The no EH policy eliminates the optimization of energy harvesting time and instead relies on fixed power supplies at both local UDs and the UAV for task processing.

Fig. 3 illustrates the convergence of total system energy consumption vs. iteration count. The proposed scheme demonstrates rapid convergence, reaching the optimal value within merely four iterations, which confirms the consistent availability of the joint optimal solution (caching, energy harvesting, offloading, and STAR-RIS resource allocation). Moreover, it exhibits a slightly faster convergence speed and ultimately a lower total energy consumption compared to all benchmark schemes, verifying the energy efficiency superiority of our ASTAR-RIS and WPT-assisted framework for WSNs.

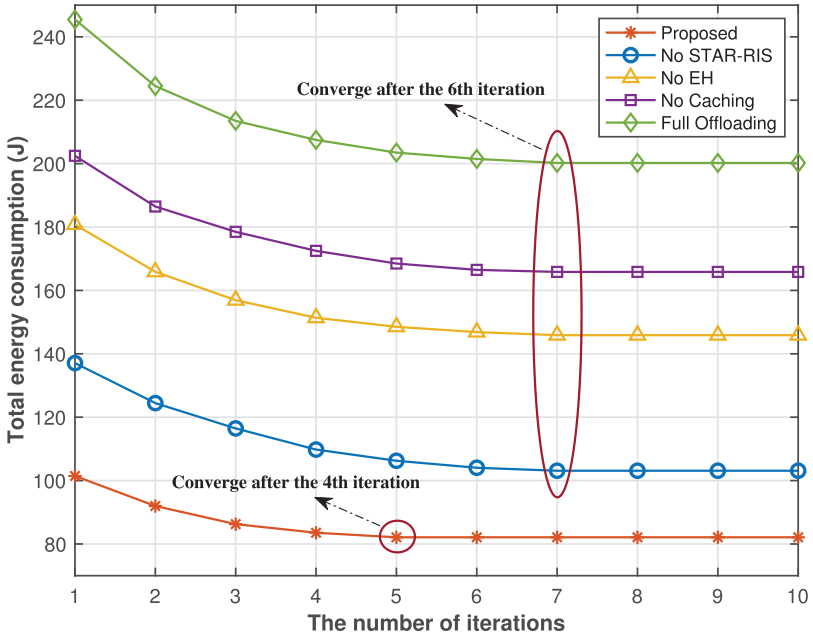

Figure 3: Total energy consumption vs the number of iterations.

Fig. 4 illustrates that the total energy consumption across all considered schemes increases significantly with the BS's enhanced computational capacity. While a more powerful BS accelerates task processing, the unchanged offloading ratio leads to a substantial rise in energy consumption for remote centralized computing, thereby driving the overall increase. As a result, when the offloading proportion is fixed, the overall energy consumption grows with the increase in BS computation capacity. At lower BS capacities, our proposed joint optimization strategy, which integrates caching, energy harvesting, partial offloading, and STAR-RIS beamforming, shows a minor performance gap relative to benchmarks while consistently

maintaining optimal system performance. As BS capacity grows, remote computing energy becomes the dominant contributor to total consumption. Under these circumstances, our proposed solution's synergy of caching optimization, energy harvesting, and partial offloading effectively curbs the steep rise in remote centralized computing energy consumption, causing the performance gap with the "No Caching", "No EH", and "Full Offloading" schemes to widen significantly. By contrast, its advantages over the "no STAR-RIS" scheme remain almost unchanged, because the proposed STAR-RIS passive beamforming strategy mainly affects the transmission energy from UDs to the distant BS but does not affect the energy consumption of remote computing. Consequently, as the BS computation power increases, the gap between our solution and the "No STAR-RIS" benchmark remains nearly constant.

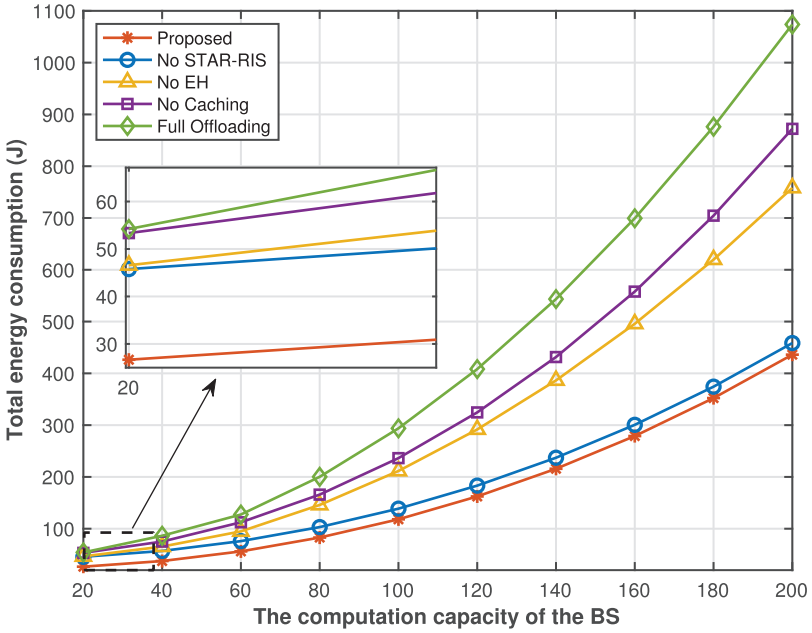

Figure 4: Total energy consumption vs the computation capacity of the BS.

Fig. 5 illustrates that, as the number of CPU cycles required to process one bit of task data increases, more computing resources are needed to handle tasks of a fixed size, which in turn leads to a marked rise in computation-related energy consumption. Under limited computing capability at the UAV and UDs, a larger portion of tasks is offloaded to the remote BS, thereby further increasing both long-distance transmission energy and centralized computing energy. As the offloaded tasks grow, network resources become progressively more constrained. Under such resource-constrained conditions, our proposed joint strategy proves effective in significantly curbing the associated energy costs of long-distance transmission and remote centralized computing compared to baseline schemes. Consequently, the energy efficiency gap between our solution and the baseline schemes widens progressively.

Fig. 6 depicts the convergence behavior of the DRL-caching agent's average weighted reward under different learning rates. It can be observed that the agent attains fast convergence in all cases, with the best overall performance achieved when the learning rate is set to 0.0003. When the learning rate is too large, temporal-difference errors have an excessive influence on critic updates, which may undermine the stability of the actor's policy improvement. In contrast, an overly small learning rate slows down the propagation of value estimates through the neural network, resulting in sluggish learning dynamics. These results highlight

that a proper choice of learning rate is essential to strike a balance between convergence speed and training stability, and thus to obtain satisfactory performance.

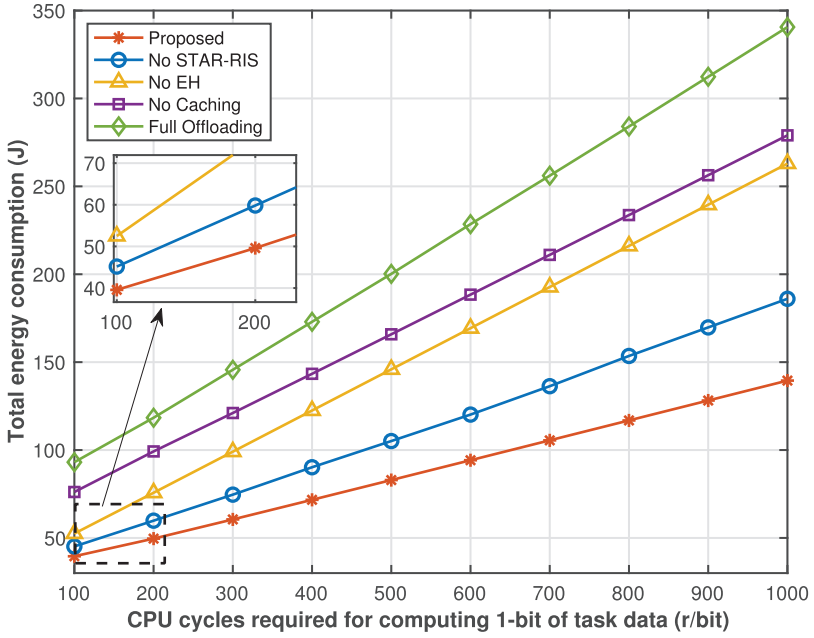

Figure 5: Total energy consumption vs a function of CPU cycles per Bit.

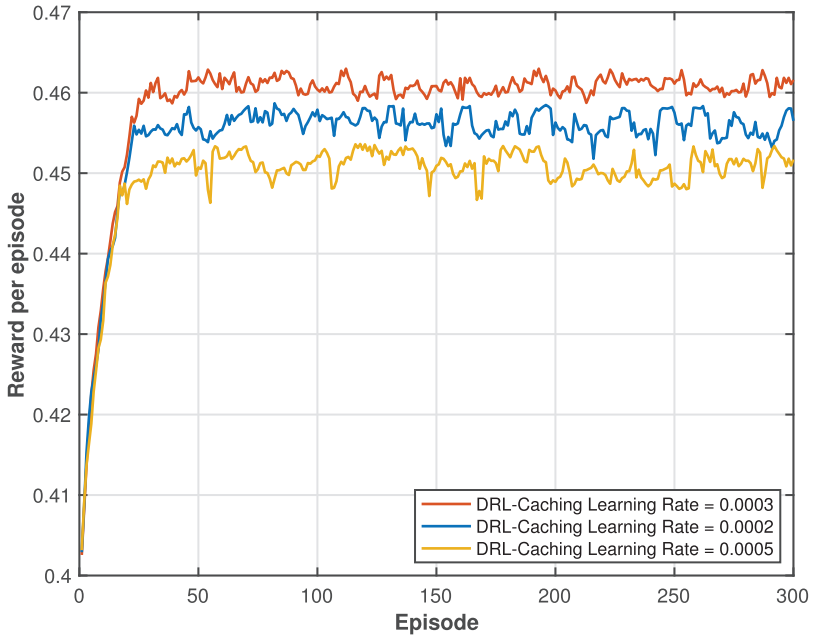

Figure 6: Average cumulative weighted reward vs different learning rates of the caching DRL agent.

7 Conclusions

In this paper, we propose an energy-efficient ASTAR-RIS and WPT-assisted task offloading and content caching framework to address the problems that restrict UAV endurance, underutilized network caching and

computing resources, and inefficient resource allocation in WSNs. In this framework, by integrating WPT for continuous energy harvesting and mounting STAR-RIS on the UAV, energy efficiency is optimized, extending UAV endurance and improving task processing efficiency. Furthermore, we construct a minimization problem that jointly optimizes content caching, energy harvesting time, task offloading, and STAR-RIS resource allocation decisions to minimize energy consumption. To address the non-convex problem of system energy consumption minimization, a joint DRL–SCA–based algorithm is designed, which iteratively achieves the solution and attains near-optimal performance with relatively low computational complexity. Simulation results show that the proposed framework substantially lowers the total energy consumption in WSNs while achieving a rapid convergence behavior.

As an important direction for future work, we will consider extending the proposed framework to jointly optimize the UAV hovering location together with WPT-enabled energy harvesting, caching, offloading, and STAR-RIS configuration to further improve system energy efficiency. Furthermore, regarding UD scalability, the proposed framework can accommodate a practical number of UDs. However, as the number of UDs increases, resource contention becomes more severe, and the energy and latency constraints may tighten, which calls for careful performance–complexity trade-offs. For large-scale deployments, hierarchical optimization and multi-UAV cooperative architectures are promising directions for future work. From a practical implementation perspective, the proposed framework is compatible with current UAV, WPT, and STAR-RIS hardware technologies. As another important direction for future work, we will conduct prototype-based evaluations and field trials to assess the performance under practical hardware limitations. The last promising direction is the integration of additional renewable energy sources, such as solar power, to create hybrid energy harvesting systems. Solar-powered UAVs can extend operational endurance during daytime missions, while RF-WPT provides consistent energy availability regardless of lighting conditions. The joint optimization of multi-source energy harvesting, along with caching, offloading, and STAR-RIS configuration, presents an exciting avenue for future research toward fully sustainable WSN deployments.

Acknowledgement: Not applicable.

Funding Statement: This research was funded by the National Social Science Foundation of China (22CGL017).

Author Contributions: The authors confirm contribution to the paper as follows: study conception and design: Xiaoping Yang; data collection: Junqi Long; analysis and interpretation of results: Songjie Yang and Xiaoping Yang; draft manuscript preparation: Xiaoping Yang, Quanzeng Wang and Bin Yang; visualization: Guochao Qi; project administration and funding acquisition: Xiaofang Cao. All authors reviewed and approved the final version of the manuscript.

Availability of Data and Materials: The data used to support the findings of this study are available from the corresponding author upon request.

Ethics Approval: Not applicable.

Conflicts of Interest: The authors declare no conflicts of interest.

References

1. Shen J, Wang A, Wang C, Hung PCK, Lai CF. An efficient centroid-based routing protocol for energy management in WSN-assisted IoT. IEEE Access. 2017;5:18469–79. doi:10.1109/access.2017.2749606.
2. Chettri L, Bera R. A comprehensive survey on Internet of Things (IoT) toward 5G wireless systems. IEEE Internet Things J. 2020;7(1):16–32. doi:10.1109/jiot.2019.2948888.
3. Ji J, Zhu K, Yi C, Niyato D. Energy consumption minimization in UAV-assisted mobile-edge computing systems: joint resource allocation and trajectory design. IEEE Internet Things J. 2021;8(10):8570–84.

4. Liao Z, Yin G, Tang X, Liu P. A cooperative community-based framework for service caching and task offloading in multi-access edge computing. IEEE Trans Netw Serv Manage. 2024;21(3):3224–35. doi:10.1109/tnsm.2024.3372295.
5. Zhang K, Gui X, Ren D, Li D. Energy latency tradeoff for computation offloading in UAV-assisted multiaccess edge computing system. IEEE Internet Things J. 2021;8(8):6709–19. doi:10.1109/jiot.2020.2999063.
6. Gao X, Zhu X, Zhai L. AoI-sensitive data collection in multi-UAV-assisted wireless sensor networks. IEEE Trans Wireless Commun. 2023;22(8):5185–97. doi:10.1109/twc.2022.3232366.
7. Duo B, He M, Wu Q, Zhang Z. Joint dual-UAV trajectory and RIS design for ARIS-assisted aerial computing in IoT. IEEE Internet Things J. 2023;11(10):17249–63. doi:10.1109/jiot.2023.3288213.
8. Xiao H, Hu X, Wang W, Su Z, Wong KK, Yang K. STAR-RIS and UAV combination in MEC networks: simultaneous task offloading and communications. IEEE Trans Commun. 2025;73(8):6169–84.
9. Wu C, You C, Liu Y, Gu X, Cai Y. Channel estimation for STAR-RIS-Aided wireless communication. IEEE Commun Lett. 2022;26(3):652–6. doi:10.1109/lcomm.2021.3139198.
10. Xiao H, Hu X, Mu P, Wang W, Zheng TX, Wong KK, et al. Simultaneously transmitting and reflecting RIS (STAR-RIS) assisted multi-antenna covert communication: analysis and optimization. IEEE Trans Wireless Commun. 2024;23(6):6438–52. doi:10.1109/twc.2023.3331706.
11. Aung PS, Nguyen LX, Tun YK, Han Z, Hong CS. Aerial STAR-RIS empowered MEC: a DRL approach for energy minimization. IEEE Wireless Commun Lett. 2024;13(5):1409–13.
12. Singh CK, Kumar D, ki Lehtom J, Khan Z, Latva-Aho M, Upadhyay PK. Robust UAV-integrated active STAR-RIS RSMA networks: analysis with deep learning techniques. IEEE Trans Veh Technol. 2025;74(5):8297–302.
13. Zhai Z, Dai X, Duo B, Wang X, Yuan X. Energy-efficient UAV-mounted RIS assisted mobile edge computing. IEEE Wireless Commun Lett. 2022;11(12):2507–11. doi:10.1109/lwc.2022.3206587.
14. Ye Y, Shi L, Chu X, Hu RQ, Lu G. Resource allocation in backscatter-assisted wireless powered MEC networks with limited MEC computation capacity. IEEE Trans Wireless Commun. 2022;21(12):10678–94. doi:10.1109/twc.2022.3185825.
15. Li J, Dai M, Su Z. Energy-aware task offloading in the Internet of Things. IEEE Wireless Commun. 2020;27(5):112–7. doi:10.1109/mwc.001.1900495.
16. Xu Y, Zhang T, Liu Y, Yang D, Xiao L, Tao M. UAV-assisted MEC networks with aerial and ground cooperation. IEEE Trans Wireless Commun. 2021;20(12):7712–27. doi:10.1109/twc.2021.3086521.
17. Zhou R, Wu X, Tan H, Zhang R. Two time-scale joint service caching and task offloading for UAV-assisted mobile edge computing. In: Proceedings of the IEEE INFOCOM 2022—IEEE Conference on Computer Communications; 2022 May 2–5; London, UK.
18. Yang Z, Chen M, Liu X, Liu Y, Chen Y, Cui S, et al. AI-driven UAV-NOMA-MEC in next generation wireless networks. IEEE Wireless Commun. 2021;28(5):66–73. doi:10.1109/mwc.121.2100058.
19. Liu Z, Li Z, Wen M, Gong Y, Wu YC. STAR-RIS-aided mobile edge computing: computation rate maximization with binary amplitude coefficients. IEEE Trans Commun. 2023;71(7):4313–27. doi:10.1109/tcomm.2023.3274137.
20. Eghbali Y, Mohammadisarab A, Zarini H, Mili MR, Basar E, Renzo MD, et al. Integrated sensing and communication for STAR-RIS-Aided UAV networks. IEEE Trans Veh Technol. 2025;74(7):11638–43. doi:10.1109/tvt.2025.3546544.
21. Chaudhary S, Nehra A, Budhiraja I, Chaudhary R, Bansal A. STAR-RIS based resource scheduling and mode selection for drone assisted 5G communications. In: Proceedings of the IEEE INFOCOM 2024 IEEE Conference on Computer Communications Workshops (INFOCOM WKSHPS); 2024 May 20–24; Vancouver, BC, Canada.
22. Yang D, Li B, Niyato D. Energy-aware task offloading for rotatable STAR-RIS-enhanced mobile edge computing systems. IEEE Internet Things J. 2025;12(12):20239–50. doi:10.1109/jiot.2025.3542463.
23. Li B, Yang D, Liu L, Niyato D. Aerial RIS-enhanced communications: joint UAV trajectory, altitude control, and phase shift design. IEEE Trans Wireless Commun. 2025;25:5830–45.
24. Budhiraja I, Vishnoi V, Kumar N, Garg D, Tyagi S. Energy-efficient optimization scheme for ris-assisted communication underlaying UAV with NOMA. In: Proceedings of the ICC 2022 IEEE International Conference on Communications; 2022 May 16–20; Seoul, Republic of Korea.

25. Mu X, Liu Y, Guo L, Lin J, Schober R. Simultaneously transmitting and reflecting (STAR) RIS aided wireless communications. IEEE Trans Wireless Commun. 2022;21(5):3083–98. doi:10.1109/twc.2021.3118225.
26. Zhou F, Hu RQ. Computation efficiency maximization in wireless-powered mobile edge computing networks. IEEE Trans Wireless Commun. 2020;19(5):3170–84.
27. Huang L, Bi S, Zhang YJA. Deep reinforcement learning for online computation offloading in wireless powered mobile-edge computing networks. IEEE Trans Mob Comput. 2020;19(11):2581–93. doi:10.1109/tmc.2019.2928811.
28. Yang X, Wang Q, Yang B, Cao X. Energy-efficient aerial STAR-RIS-aided computing offloading and content caching for wireless sensor networks. Sensors. 2025;25(2):393. doi:10.3390/s25020393.
29. Luo Y, Ding W, Zhang B. Optimization of task scheduling and dynamic service strategy for multi-UAV-enabled mobile-edge computing system. IEEE Trans Cogn Commun Netw. 2021;7(3):970–84. doi:10.1109/tccn.2021.3051947.
30. Alotaibi J, Oubbati OS, Atiquzzaman M, Alromithy F, Altimania MR. Optimizing disaster response with UAV-mounted RIS and HAP-enabled edge computing in 6G networks. J Netw Comput Appl. 2025;241(4):104213. doi:10.1016/j.jnca.2025.104213.
31. Chen J, Xing H, Xiao Z, Xu L, Tao T. A DRL agent for jointly optimizing computation offloading and resource allocation in MEC. IEEE Internet Things J. 2021;8(24):17508–24. doi:10.1109/jiot.2021.3081694.
32. Xu J, Liu Y, Mu X, Dobre OA. STAR-RISs: simultaneous transmitting and reflecting reconfigurable intelligent surfaces. IEEE Commun Lett Sep. 2021;25(9):3134–8. doi:10.1109/lcomm.2021.3082214.
33. Ameur AI, Oubbati OS, Rachedi A, Arishi A, Atiquzzaman M. Intelligent UAV caching and energy management in 6G networks. IEEE Trans Netw Sci Eng. 2026;13:3175–92. doi:10.1109/tnse.2025.3628171.
34. Su Y, Pang X, Lu W, Zhao N, Wang X, Nallanathan A. Joint location and beamforming optimization for STAR-RIS aided NOMA-UAV networks. IEEE Trans Veh Technol. 2023;72(8):11023–8. doi:10.1109/tvt.2023.3261324.
35. Lin N, Bai L, Hawbani A, Guan Y, Mao C, Liu Z, et al. Deep-reinforcement-learning-based computation offloading for servicing dynamic demand in multi-UAV-assisted IoT network. IEEE Internet Things J. 2024;11(10):17249–63. doi:10.1109/jiot.2024.3356725.
36. Zhang Q, Zhao Y, Li H, Hou S, Song Z. Joint optimization of STAR-RIS assisted UAV communication systems. IEEE Wireless Commun Lett. 2022;11(11):2390–4. doi:10.1109/lwc.2022.3204353.